Kinetic Modeling of [^{99m}Tc]TRODAT-1: A Dopamine Transporter Imaging Agent

Steven A. Kushner, William T. McElgin, Mei-Ping Kung, P. David Mozley, Karl Plössl, Sanath K. Meegalla, Mu Mu, Stefan Dresel, Janet M. Vessotskie, Nedra Lexow and Hank F. Kung

Departments of Radiology and Psychiatry, University of Pennsylvania, Philadelphia, Pennsylvania

[^{99m}Tc]Technetium[2-[[2-[[[3-(4-chlorophenyl)-8-methyl-8-azabicyclo [3.2.1] oct-2-yl]-methyl] (2-mercaptoethyl) amino] ethyl] amino] ethane-thiolato(3-)-*N2,N2',S2,S2'*]oxo-[1*R*-(exo-exo)] ([^{99m}Tc] TRODAT-1) is a useful imaging agent for central nervous system dopamine transporters. The purpose of this study was to characterize the in vivo binding potential and kinetic rate constants of this agent in nonhuman primates. **Methods:** A series of four SPECT scans were performed on each of two female baboons with a bolus injection of [^{99m}Tc]TRODAT-1 (717 ± 78 MBq; 19.38 ± 2.12 mCi). Dynamic images of the brain were acquired over 4 h using a triple-head camera equipped with fan-beam collimators. Arterial and venous blood were sampled frequently using a peristaltic pump throughout the duration of the study. Regions of interest were drawn on the corresponding MRI scan to which each functional image was coregistered. Using analytical solutions to the three-compartment model with the Levenberg-Marquardt minimization technique, each study was individually fitted to a kinetic parameter vector (method I). Additionally, within each subject, three corresponding intrasubject studies were fitted simultaneously to a single parameter vector by constraining the binding potential, distribution volume and dissociation rate constant to improve the identifiability of the parameter estimates (method II). **Results:** The results clearly indicated that [^{99m}Tc] TRODAT-1 localized in the striatum with slower washout rate than other brain regions. A maximal target/nontarget ratio of 3.5 between striatum and cerebellum was obtained. SPECT image analysis of the striatum yielded unconstrained k_3/k_4 values of 3.4 ± 1.4, 2.4 ± 0.7, 3.0 ± 1.5, and 4.0 ± 10.3, with respective constrained (fixed k_4) values of 2.9 ± 0.4, 2.4 ± 0.4, 1.7 ± 0.4 and 1.8 ± 0.4 in one baboon using method I. With method II, the corresponding simultaneously fitted values were 2.1 ± 0.3 using no constraints and 2.2 ± 0.2 using a fixed k_4. The second baboon had similar results. **Conclusion:** These findings suggest that the binding potential and corresponding kinetic rate constants can be reliably estimated in nonhuman primates with dynamic SPECT imaging of the dopamine transporter using a technetium-based tropane analogue. Furthermore, method II parameter vectors compare favorably to those produced using method I based on SEEs.

Key Words: striatum; SPECT; dopamine neuron; Parkinson's disease

J Nucl Med 1999; 40:150–158

Received Oct. 21, 1997; revision accepted Apr. 28, 1998.

For correspondence or reprints contact: Hank F. Kung, PhD, Department of Radiology, University of Pennsylvania, 3700 Market St., Room 305, Philadelphia, PA 19104.

The dopamine transporter (DAT) protein, located on presynaptic dopamine neuron terminals, is principally involved in the regulation of synaptic dopamine levels by a reuptake mechanism (*1*). The striatum is a dopamine-rich region and consequently has high densities of presynaptic DATs (*2*). In mice lacking the gene for the dopamine transporter, spontaneous hyperlocomotion results despite adaptive changes such as decreases in dopamine and postsynaptic receptor levels (*3*). As a result of its significant role in dopamine regulation, the DAT protein is a targeted binding site for various psychoactive drugs, including cocaine and amphetamines (*4*).

A large number of DAT imaging agents, based on cocaine or its closely related congeners tropane derivatives, have been reported as useful PET and SPECT imaging agents. These agents include [^{11}C]*N*-methyl–labeled cocaine (*5*), [^{11}C]2β-carboxymethoxy-3β-(4-fluorophenyl)tropane (CFT) (WIN35,428) (*6,7*), [^{11}C]methylphenidate (*8*), [^{123}I]β-2β-carboxymethoxy-3β-(4-iodophenyl)tropane (CIT) (*9,10*), [^{123}I]N-(3′-iodopropen-2′-yl)-2β-carbomethoxy-3β-(4-chlorophenyl) (IPT) (*11,12*), [^{123}I]CIT-N-(3′-fluoropropyl) (FP) (*13,14*) and [^{123}I]altropane (*15*). Agents for both PET and SPECT imaging have shown excellent specific uptake in the striatum and have been useful in evaluating changes in dopamine reuptake sites in vivo and in vitro, especially for patients with Parkinson's disease, which is characterized by a selective loss of dopaminergic nigrastriatal neurons (*6,7,16*). To improve the availability of SPECT imaging agents for studying DATs on a routine basis, there is a need for ^{99m}Tc-based compounds. ^{99m}Tc ($t_{1/2}$ = 6 h; 140 KeV) is the most commonly used radionuclide in diagnostic nuclear medicine (*17*). The development of ^{99m}Tc-based small molecules as receptor imaging agents has been reviewed recently (*18*). In developing ^{99m}Tc-labeled DAT imaging agents, several ^{99m}Tc-labeled tropanes have been reported (*19–22*), among which the specific binding of [^{99m}Tc]technetium[2-[[2-[[[3-(4-chlorophenyl)-8-methyl-8-azabicyclo-[3.2.1]oct-2-yl]-methyl](2-mercaptoethyl)amino]-ethyl]-amino]ethane-thiolato(3-)-*N2,N2',S2,S2'*]oxo-[1*R*-(exo-exo)] ([^{99m}Tc]TRODAT-1) to DAT protein located in the basal ganglia area of the human brain has been the most promising agent (*23*). [^{99m}Tc]TRODAT-1 has been shown to bind with

high selectivity to the basal ganglia, specifically to the caudate and putamen (*21,23,24*). Specific uptake of [^{99m}Tc]-TRODAT-1 can be inhibited by coadministering animals with pharmacological doses of competing compounds. Using dynamic SPECT, the distribution of [^{99m}Tc]TRODAT-1 within the brain can be examined over short time intervals, and kinetic parameters can be estimated.

The influence of regional cerebral blood flow and tracer peripheral clearance on outcome measures, such as the striatal/background ratio, remains unclear in nonequilibrium conditions (*25*). Compartmental kinetic modeling studies (*26,27*) using the high-affinity [^{11}C]CFT and [^{123}I]β-CIT have been used previously to estimate receptor parameters independent of regional cerebral blood flow and tracer peripheral clearance (*6,10*). Using similar model-based methods that require arterial input functions and dynamic SPECT acquisitions, the in vivo kinetics of [^{99m}Tc]TRODAT-1 were examined together with ex vivo comparisons in nonhuman primates, and the results are reported herein.

MATERIALS AND METHODS

Radiolabeling

The labeling procedure used was reported previously (*21,24*). Briefly, a dried sample of TRODAT-1 (200 μg TRODAT-1) was dissolved in 100 μL ethanolic HCl (100 μL HCl [2N] in 2 mL ethanol) and 200 μL HCl (2N). To this solution, 50 μL of a sodium ethyldiaminetetraacetic acid solution (0.05 mol/L) and 800 μL tin-glucoheptonate solution (40 μg $Sn(II)Cl_2$ and 400 μg sodium glucoheptonate per milliliter of solution) were added, followed by 100–200 μL of [^{99m}Tc]pertechnetate solution (in a range of 20–40 mCi) and 500 μL water. The vial was autoclaved for 30 min. After cooling to room temperature, phosphate buffer (500 μL, pH 6–7) was added. The radiochemical purity was determined by reversed-phase high-performance liquid chromatography (HPLC) analysis on a PRP-1 column (250 × 4.1 mm; Hamilton Co., Reno, NV) eluting with acetonitrile/3,3-dimethylglutaric acid (DMGA) buffer (pH 7) in a ratio of 80:20 and a flow rate of 1 mL/min. The retention time of [^{99m}Tc]TRODAT-1 was 13–15 min under these conditions. Radiochemical purity was equal to 90%, and this purity was suitable for imaging studies.

SPECT Acquisition and Analysis

A series of four dynamic SPECT scans were performed on each of two female olive baboons (*Papio anubis*) under protocols approved by the Institutional Review Board and the local animal care committee. The interval between each successive scan was at least 2 wk. After overnight fasting, animals were immobilized with a combined intramuscular injection of 10 mg/kg ketamine and 2 mg/kg xylazine. During the scanning procedure, anesthesia was maintained by passive inhalation of 1.8% isoflurane (1.2 L O_2/min). An intravenous line in a superficial cephalic vein allowed for hydration (0.9% NaCl, 5 mL/kg/h) as well as for ligand administration. A cylindrical polycarbonate positioning device equipped with a customized foam head holder enabled reproducible placement of the animal in the SPECT camera. The core body temperature was maintained using a circulating warm water pad maintained at 37°C. A single bolus injection (717 ± 78 MBq; 19.38 ± 2.12 mCi) of [^{99m}Tc]TRODAT-1 was administered immediately before each scan. The specific activity of [^{99m}Tc]TRODAT-1 was ≥100 Ci/μmol. We assumed that the pseudocarrier did not contribute significantly to the chemical amount in the specific activity estimation.

A total of 42 dynamic images of the brain were acquired over 4 h using a triple-head SPECT camera equipped with fanbeam collimators (Prism 3000; Picker International, Cleveland, OH). During the first 30 min, acquisitions were made every 2 min for a total of 15 image sets. Between 30 and 90 min postinjection, 12 acquisitions were performed in 5-min intervals. During the final 150 min, images were acquired in 10-min frames. The acquisition parameters included a 14-cm rotational radius and a symmetric 15% ^{99m}Tc energy window at 140 KeV to produce a volume of 128 × 128-pixel matrices. Both the slice thickness and in-plane pixel size were 2.0 mm in the projection data. The images were reconstructed with a low-pass filter and corrected for attenuation. No attempt was made to correct for partial volume effects.

Radioactivity in the [^{99m}Tc]TRODAT-1/SPECT scans was localized using the corresponding MR image for the animal. The MR images were acquired on a 1.5-T instrument (GE Medical Systems, Milwaukee, WI) with a spoiled MRI pulse sequence that produces 0.97 × 0.97 × 1-mm voxels. The MR images were resized and resliced in planes parallel to the one containing the anterior and posterior commissures. Regions of interest (ROIs) for the basal ganglia, cerebellum and cerebral hemispheres were drawn directly onto the MR image inside the outer edge of each structure to minimize the effects of volume averaging. Coregistration of the SPECT scans and the MR images was achieved using a customized software package developed to rotate and translate each SPECT scan with respect to a fixed MRI data set (*28*). Fusion images of SPECT and MRI were generated to visually validate the accuracy of the coregistration in the sagittal, coronal and transverse planes.

Once each SPECT scan was coregistered with the MR image, the ROIs were transposed identically and unaltered onto each [^{99m}Tc]TRODAT-1/SPECT image as a single set. The mean counts per pixel in these regions were measured for each functional scan. Counts in the reconstruction domain were converted to microcuries per milliliter with experimentally measured calibration factors for the camera obtained by imaging uniform phantoms that contained known concentrations of radioactivity. The absolute activities were used to compute the mean fraction of the injected dose per unit volume.

Blood Sampling

During each SPECT protocol, in-dwelling arterial and venous catheters were positioned, and blood samples were collected to monitor the plasma concentration of unmetabolized [^{99m}Tc] TRODAT-1 ($C_A(t)$). Arterial catheters were placed in the popliteal artery, and venous catheters were placed in the contralateral saphenous vein. Arterial and venous blood sampling occurred simultaneously over the first 5 min (8.4 s per sample) using an automatic peristaltic pump (Gilson, Inc., Middleton, WI). Subsequent sampling was performed manually at 6, 10, 15, 30, 60, 90, 120, 150, 180 and 240 min postinjection.

Metabolite Analysis

Heparinized blood samples were centrifuged at 1000*g* for 10 min. The radioactivity in separated plasma samples was counted in an automatic gamma-counter (Packard 5000; Packard Instrument, Meriden, CT). All of the radioactivity measurements were corrected for decay. The plasma samples were extracted with ethyl

acetate (3 × 1.5 mL) in the presence of Re-TRODAT-1 complex (100 μg) after adjusting the pH to 8.0 with phosphate buffer. Extraction was calculated from the activity in the organic and aqueous layers. The ethyl acetate layers were evaporated to near dryness, and the radioactive profile was analyzed by HPLC on a PRP-1 column (Hamilton Co.; 4.1 × 250 mm) eluted with a solvent mixture of CH_3CN/DMGA buffer (pH 7.0):8/2 and a flow rate of 1.5 mL/min. Controls were determined by adding 10–20 μCi [^{99m}Tc]TRODAT-1 to the plasma followed by the same procedures used for the experimental samples to determine the extraction efficiency. The unmetabolized [^{99m}Tc]TRODAT-1 in the plasma samples ($C_A(t)$) can thus be calculated from the fraction extracted and the parent composition (HPLC), divided by a recovery coefficient. The recovery coefficient is computed as the product of the extraction and fraction of [^{99m}Tc]TRODAT-1 in control samples.

Protein Binding

The binding of [^{99m}Tc]TRODAT-1 to plasma proteins in vitro was determined by ultrafiltration through Centricon-30 membrane filters (Amicon Division, W.R. Grace & Co., Danves, MA). The membranes were prewetted with cold TRODAT-1 (1 μg/mL). Initially, 10 μL diluted [^{99m}Tc]TRODAT-1 (1:100; vol/vol) and 10 μL TRODAT-1 free thiol ligand (1 mg/100 μL) were added to 0.7 mL each of plasma (obtained from venous blood sample) and normal saline (as control). Duplicate samples of 200 μL were placed in the unit and centrifuged at 3500 rpm for 10 min at room temperature. The protein-bound fraction (f_1) was calculated as the ratio of the radioactivity on the filter to the sum of the filter and the filtrate. The plasma-free fraction ($f_1 = C_P(t)/C_A(t)$) (*29*) computed for each animal was assumed to be constant over the course of each experiment.

The free parent plasma concentration for each study was fit to a sequence of two functions. Between $t = 0$ and the time ($t_1 = 1.70 \pm 0.11$ min) of the peak measured value, a linear function was used. In the interval $t > t_1$, a sum of n exponentials was used to fit the data as follows:

$$C_P(t) = f_1 C_A(t) = f_1 \sum_{i=1}^{n} A_i e^{-\lambda_i t}, \qquad \text{Eq. 1}$$

where for each exponential in the sum, λ_i (min^{-1}) was the decay constant of each exponential and $A_i e^{-\lambda_i t}$ (in μCi/mL) was the peak of each exponential.

Ex Vivo Cerebral Biodistribution

Post mortem dissection was performed immediately after the last image of the last scan in one of the baboons 240 min after the administration of [^{99m}Tc]TRODAT-1. The brain was excised and dissected into regions that include the striatum, cerebellum, hippocampus, thalamus, frontal cortex and occipital cortex. Each tissue sample was transferred into preweighed culture tubes and weighed. The amount of radioactivity in each sample was calculated from the number of counts measured in a well counter for 1 min. The counts were corrected for decay to the time of death of the animal. The concentration of radioactivity in microcuries per gram was calculated from the counts per minute per gram with an experimentally measured calibration factor for the well counter.

In Vivo Kinetic Analysis

It is assumed that the in vivo kinetics of [^{99m}Tc]TRODAT-1 followed a three-compartment model (Fig. 1) in which C_1 represented the sum of the nonspecifically bound and free ligand

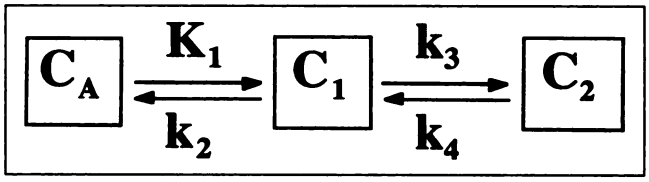

FIGURE 1. Three-compartment model consists of arterial compartment (C_A), nonspecific intracerebral compartment (C_1) and specifically bound compartment (C_2). Kinetic analysis yielded estimates of rate constants K_1 to k_4.

concentrations, C_A was the arterial concentration of nonspecifically bound and free parent ligand and C_2 was the concentration of transporter-bound ligand (*26,27*). The nonspecifically bound and free ligand concentrations within C_A and C_1 were assumed to equilibrate rapidly. Similarly to C_A, the fraction of free ligand in C_1 (f_2 = free intracerebral concentration/$C_1(t)$) was assumed to be nearly constant throughout the duration of a study.

The differential equations describing the rate of change with respect to time of the ligand concentration for each compartment are given by the following equations:

$$\frac{dC_1(t)}{dt} = K_1 C_A(t) - (k_2 + k_3) C_1(t) + k_4 C_2(t) \qquad \text{Eq. 2}$$

and

$$\frac{dC_2(t)}{dt} = k_3 C_1(t) - k_4 C_2(t). \qquad \text{Eq. 3}$$

The kinetic rate constants K_1 ($mL/g^{-1}/min^{-1}$) and k_2 (min^{-1}) represent bidirectional transport across the blood-brain barrier, where K_1 is the plasma clearance. We assumed that passive diffusion of the ligand across the blood-brain barrier was the only significant mechanism of transport in which the concentration of free ligand in the brain was equal to the free plasma concentration at equilibrium (*30,31*). The derivatives of equations 2 and 3 were set to zero:

$$f_2 = f_1 \frac{k_2}{K_1}. \qquad \text{Eq. 4}$$

The first-order rate constant k_4 is identical to the dissociation rate constant k_{off}, and k_3 is a function of the density of available binding sites:

$$k_3 = f_2 k_{on} B_{max}', \qquad \text{Eq. 5}$$

where $B_{max}' = (B_{max} - C_2(t)/SA) = B_{max}$ during tracer studies because $B_{max} >> C_2(t)$, SA is the specific activity (≥100 Ci/μmol) of the ligand and k_{on} is the ligand-receptor association rate constant.

The binding potential (BP) of a ligand-receptor interaction is defined as the ratio of B_{max} to the equilibrium dissociation constant (K_D). Using equations 4 and 5, BP can be expressed as follows:

$$BP = \frac{B_{max}}{K_D} = \frac{K_1 k_3}{k_2 k_4 f_1}. \qquad \text{Eq. 6}$$

The total integrated ligand concentration in the blood was computed using the measured input function and contributed negligibly (<0.1%) to the regional brain activity. Therefore, the

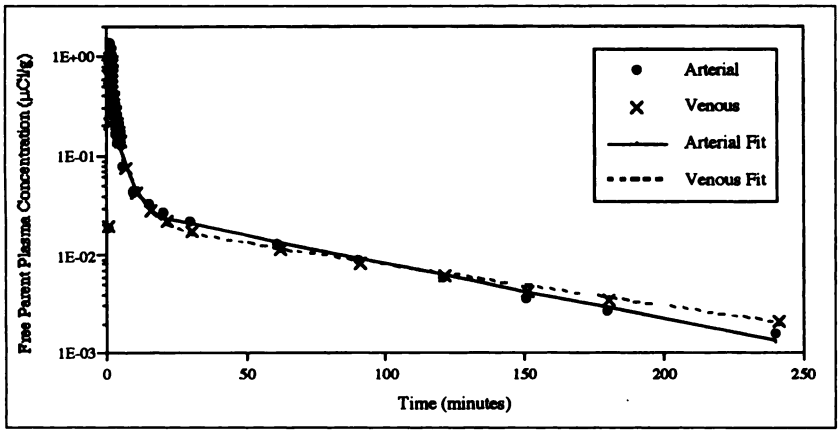

FIGURE 2. Clearance of free parent [^{99m}Tc]-TRODAT-1 from plasma was examined in both arterial and venous blood. Representative arterial and venous curves were fit to sum of four exponentials.

observed SPECT concentration of activity in an ROI was assumed to have contributions from only C_1 and C_2 (*29*).

$$C_{ROI}(t) = C_1(t) + C_2(t). \quad \text{Eq. 7}$$

Equations 2 and 3 can be solved analytically for $C_{ROI}(t)$ as the convolution of $C_A(t)$ with the impulse-response function, a sum of n exponentials (*32*). For the three-compartment model, the impulse-response function has n = 2 exponentials, corresponding to the two intracerebral compartments C_1 and C_2. The plasma clearance parameters (A_i and λ_i) and kinetic rate constant vector (K_1 to k_4) were estimated using nonlinear regression with the Levenberg-Marquart least-squares minimization algorithm (*33*).

Two different methods for estimating the in vivo BP for each subject were applied. Method I (individualized parameter fitting) involved the computation of a separate kinetic rate constant vector and BP for each individual SPECT imaging session with no a priori constraints on any parameters. Method II (simultaneous fitting) involved the computation of an overall BP by fitting the 3-compartment model simultaneously to three studies for a given subject. The blood flow parameter (K_1) was estimated independently for each study. Because we assumed that passive diffusion across the blood-brain barrier was the only significant mechanism for ligand transport, the partition coefficient (K_1/k_2) was assumed to be intrinsic to the blood-brain barrier and constrained to be constant across all studies within a given subject. The dissociation rate constant (k_4) and BP were assumed to be intrinsic to the receptor-ligand interaction, time independent and flow independent. Consequently, k_4 and BP were also constrained to be constant across all intrasubject studies. In addition to applying methods I and II with no a priori constraints, we examined the potential for poorly identified k_4 values to affect the estimation of the remaining kinetic parameters by using a fixed value of k_4. The fixed value of k_4 = 0.004 min^{-1} was chosen post hoc based on results of the method II analysis. Both subjects had very similar k_4 values (0.0044 ± 0.0017 and 0.0039 ± 0.0027 for baboons A and B, respectively) using method II in three intrasubject studies.

RESULTS

Plasma Clearance and Metabolite Analysis

The clearance of free unmetabolized parent [^{99m}Tc]TRODAT-1 from arterial and venous plasma can be examined in Fig. 2. The free fraction (f_1) in venous blood was determined by ultrafiltration method to be 12.8% ± 0.2% (n = 8). During the first 30 min postinjection, the concentration of [^{99m}Tc]TRODAT-1 activity was significantly higher in arterial blood. After 60 min postinjection, the concentration of free parent ligand in both the arterial and venous compartments was very similar. Metabolism in both arterial and venous compartments had a similar time course showing rapid degradation of the parent compound [^{99m}Tc]TRODAT-1, from >80% intact at 2 min after injection decreasing to approximately 10% unmetabolized [^{99m}Tc]TRODAT-1 remaining in both the arterial and venous bloods at 60 min after tracer injection (Fig. 3). Chromatographic profiles of radioactivity in plasma samples collected at various time

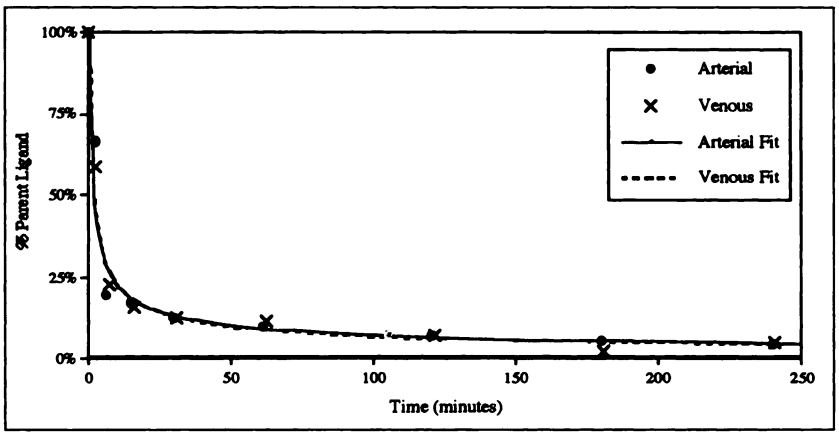

FIGURE 3. Time-dependent metabolism of [^{99m}Tc]TRODAT-1 from blood plasma was examined in both arterial and venous blood. Metabolism was very similar in both arterial and venous plasma compartments.

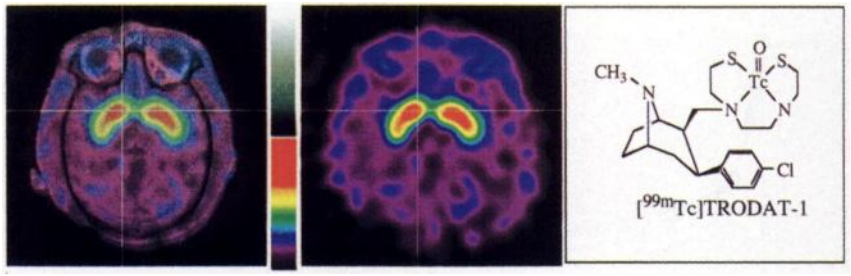

FIGURE 4. Transaxial SPECT image of brain from baboon acquired 120–180 min postinjection of 16.8 mCi [^{99m}Tc]TRODAT-1. SPECT image was coregistered with MRI image of the same baboon; this showed that agent is highly concentrated in basal ganglia area. Peak uptake occurred in basal ganglia, with target/background ratio of 3.5:1.0.

points after injection of [^{99m}Tc]TRODAT-1 indicated that, besides [^{99m}Tc]TRODAT-1, there existed a solvent-extractable polar metabolite with similar retention time on HPLC to the ^{99m}Tc-N_2S_2 moiety (data not shown).

In Vivo SPECT Analysis

The transaxial projection of SPECT studies performed in baboons showed that the regions corresponding to the caudate and putamen showed the highest concentrations of activity (Fig. 4). Total activity in the striatum peaked at 30–40 min postinjection and remained at that plateau up to 90 min, followed by slow washout from the striatal region (Fig. 5). The cerebellum, hippocampus, occipital cortex and whole brain peaked earlier and had much faster washout rates than the striatal regions (Fig. 5). Therefore, the target-to-nontarget ratios (striatum to cerebellum) increased from 1.2 at 2 min postinjection to approximately 3.5 at 4 h.

Ex Vivo Cerebral Biodistribution

The distribution of [^{99m}Tc]TRODAT-1 at 240 min postinjection of one baboon indicates preferential uptake in the striatum (Table 1). Frontal cortex, occipital cortex and cerebellum regions all had similar uptake values. The ratio of striatal-to-cerebellar uptake was 6.57, which indicates the high density of binding sites for [^{99m}Tc]TRODAT-1 in the striatum. Furthermore, a high degree of specificity of [^{99m}Tc]TRODAT-1 for the striatum is indicated by the lower background uptake (striatum-to-occipital cortex = 5.21 and striatum-to-hippocampus = 4.76). The ratio obtained with dissection (6.57) shown here is twofold higher than that observed with SPECT imaging (3.5).

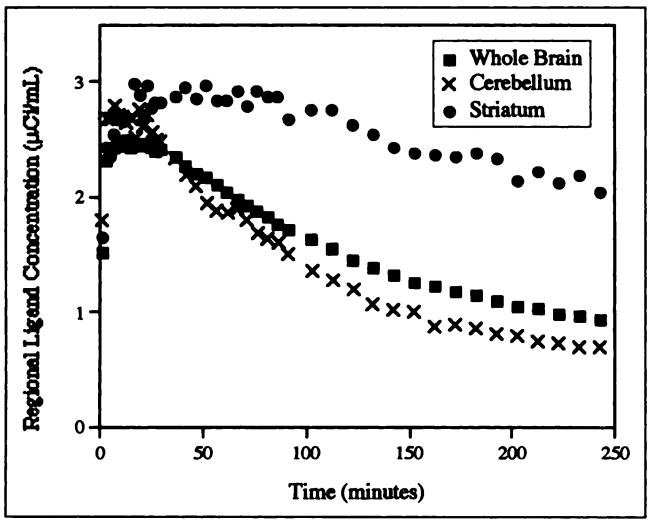

FIGURE 5. Regional time-activity curves acquired with SPECT in baboon for 4 h postinjection of 16.8 mCi [^{99m}Tc]TRODAT-1. Activity in striatum peaked at 30–40 min. Maximum target/background ratios were observed at 4 h.

Estimate of In Vivo Parameters

Using method I (individualized parameter fitting), kinetic rate constants can be estimated for each SPECT study performed with no a priori constraints on the parameters. The SPECT regional time-activity curve and the corresponding arterial plasma curve were fit to the three-compartment model. One set of full kinetic parameter vectors was calculated for each study performed. To improve the identifiability of these parameter estimates, parameter vectors were also computed using $k_4 = 0.004$ min^{-1}. Method II (simultaneous fitting) was applied to three representative studies within each baboon (baboon A: 1, 2 and 3; and baboon B: 1, 2 and 4). The three corresponding intrasubject studies were fit to a single-parameter vector by constraining the BP, distribution volume and dissociation rate constant.

Parameter and SEEs for K_1 in two baboons using methods I and II for fixed and unfixed k_4 values are shown in Fig. 6. Both methods I and II yielded a separate K_1 estimate for each study examined, because K_1 was not constrained. For the remaining estimated parameters (k_2/K_1, k_3/k_4 and k_4), method II produced only one value constrained across three intrasubject studies. In baboon A, K_1 estimates for methods I and II were very similar for corresponding studies. However, baboon B had substantially different K_1 values between methods I and II.

TABLE 1
Post-Mortem Brain Sampling of Baboon A at 240 min Postinjection of 16.7 mCi [^{99m}Tc]TRODAT-1

Region	Uptake (μCi/g)	Ratio to cerebellum
Cerebellum	0.397	1.00
Frontal cortex	0.487	1.22
Occipital cortex	0.499	1.26
Thalamus	0.476	1.20
Striatum	2.613	6.57
Hippocampus	0.547	1.38

Peak uptake was observed in the striatum (2.613 μCi/g).

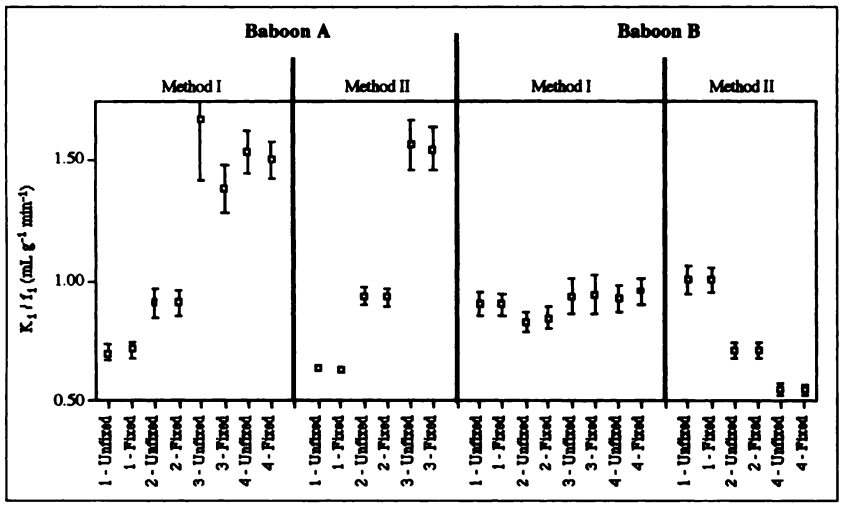

FIGURE 6. Parameter and SEEs for K_1/f_1 in two baboons using methods I and II for fixed and unfixed k_4 values. Four studies were conducted for each baboon, examined individually using method I and simultaneously using method II with three intrasubject studies. Method II yields separate K_1/f_1 estimate for each study examined.

Except for one study in baboon A (study 3), fixing k_4 had minimal effects on the parameter or SEEs. Similarly, parameter estimates of k_2/K_1 showed little variability between a fixed and unfixed k_4 except in one study (baboon A, study 3). However in a several studies, the SE decreased appreciably (Fig. 7).

The most substantial variability between different analytical methods was observed in the parameter and SEEs of k_3/k_4 (Fig. 8). Fixing k_4 substantially reduced the SE in almost every study for both methods I and II. Three studies examined using method I without fixing k_4 yielded errors that exceeded the dimensions of the graph (baboon A, study 3, 4.0 ± 10.3; baboon B, study 3, 6.5 ± 19.7; and baboon B, study 4, 4.1 ± 5.3). However, fixing k_4 in these studies yielded k_3/k_4 estimates of 1.7 ± 0.4 (baboon A, study 3), 2.2 ± 0.5 (baboon B, study 3) and 2.1 ± 0.3 (baboon B, study 4). During data collection for these three studies, some complications in SPECT data acquisition occurred related to the maintenance of anesthesia during long imaging sessions (longer than 4 h).

The dissociation parameter k_4 was poorly identified in individual studies (Fig. 9). SE measurements obtained using method II were improved compared with most studies using method I. Both subjects had very similar k_4 values (0.0044 ± 0.0017 and 0.0039 ± 0.0027 min^{-1} for baboons A and B, respectively) using method II. These results were used to assign the fixed value of k_4 = 0.004 min^{-1}, used in the analysis of the other parameters.

The variability of the BP estimates was much larger for method I than method II (Table 2). Using a fixed k_4 yielded more consistent BP estimates than values obtained using no a priori constraints. The difference between the methods I and II BP estimates was substantially decreased when k_4 was fixed for the three intrasubject studies used in both analyses.

DISCUSSION

There are numerous clinical advantages of ^{99m}Tc-labeled ligands compared with other ^{123}I-based central nervous system receptor imaging compounds. ^{99m}Tc is the most common radionuclide and is used in about 85% of routine nuclear medicine procedures (*17*). The cost of on-site manufacturing of ^{99m}Tc is <$0.30 per millicurie versus >$40 for ^{123}I. The complications of shipping an isotope over very long distances from off-site cyclotron facilities, as required for using ^{123}I, are also eliminated. Because of the

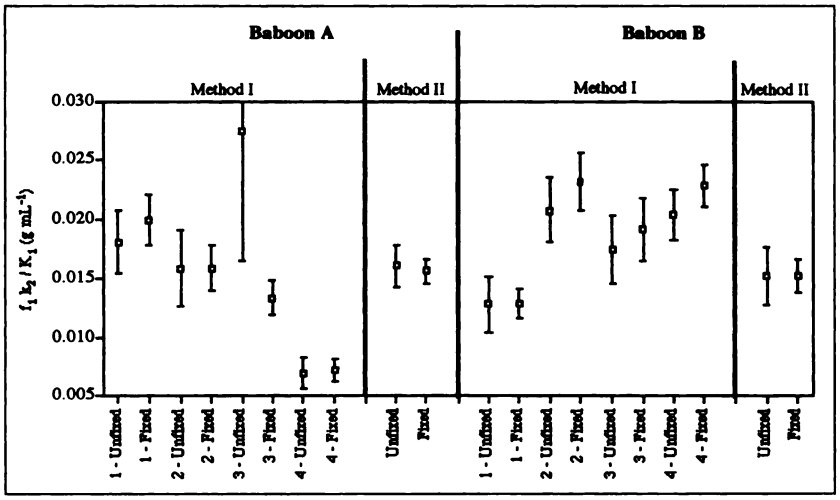

FIGURE 7. Parameter and SEEs for f_1k_2/K_1. Method II yields one value for f_1k_2/K_1, constrained across three intrasubject studies.

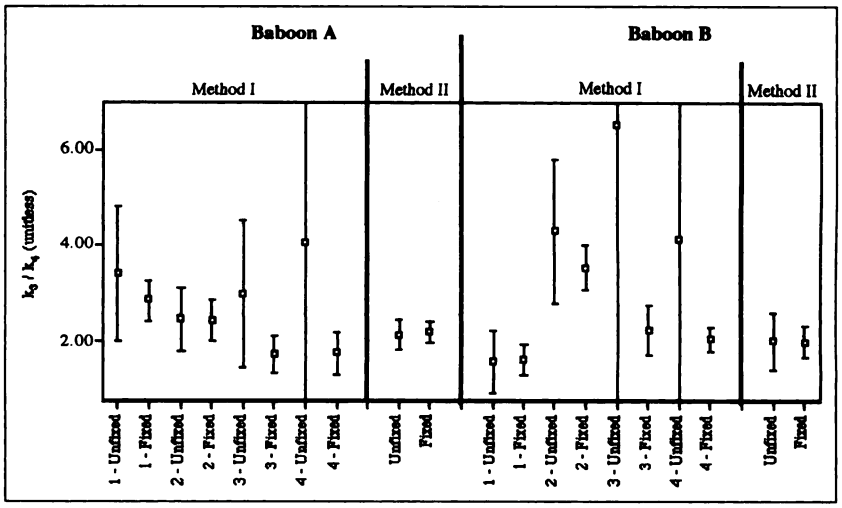

FIGURE 8. Parameter and SEEs for k_3/k_4. Method II yields one value for k_3/k_4, constrained across all intrasubject studies. Three studies examined using method I without fixing k_4 yielded errors that exceeded dimensions of graph: baboon A, study 3, 4.0 ± 10.3; baboon B, study 3, 6.5 ± 19.7; and baboon B, study 4, 4.1 ± 5.3.

shorter half-life of ^{99m}Tc, the dosimetry may also be more favorable than those ligands labeled with ^{123}I. In addition, radioiodination procedures for preparation of radiopharmaceuticals are generally more complicated and tedious than kit-based methods possible with many ^{99m}Tc-based radiopharmaceuticals, including [^{99m}Tc]TRODAT-1. There are strong incentives for developing ^{99m}Tc radiopharmaceuticals for imaging central nervous system receptors, although this goal appeared to be unattainable even a few years ago (*18*). With the success shown by [^{99m}Tc]TRODAT-1 (*23*), we have taken the next step to validate the potential of measuring DATs by in vivo SPECT imaging technique.

The results of this study establish that [^{99m}Tc]TRODAT-1 accumulates rapidly and selectively in the striatum of healthy baboons and yields high-contrast SPECT imaging at 2–3 h postinjection. Specific striatal uptake of [^{99m}Tc]TRODAT-1 can be inhibited by coadministering animals with pharmacological doses of CFT, whereas extrastriatal uptake remains unchanged. It is important to note that the striatum-to-cerebellum ratio at 4 h postinjection measured by SPECT imaging and by tissue dissection was 3.5 versus 6.6 (Table 1). The difference clearly suggests that SPECT imaging underestimates the true striatum-to-cerebellum ratio. Factors such as attenuation, scattering, partial volume effect and statistical factors may all contribute to errors in the estimate of the real activity in the ROIs.

[^{99m}Tc]TRODAT-1, the tracer used for this study, can be easily prepared within 1 h, and the preparation has been adopted for a kit formulation (*34*). From the clinical perspective, the ready availability of ^{99m}Tc compared with the iodinated tracers (i.e., [^{123}I]β-CIT and [^{123}I]IPT), will make [^{99m}Tc]TRODAT-1 even more attractive for imaging DAT. Successful human SPECT imaging performed with [^{99m}Tc]TRODAT-1 further confirmed the great potential using this ^{99m}Tc-based imaging agent for DAT protein (*23*). Structural features used in formation of neutral and lipophilic $TcO\text{-}N_2S_2$ center core and the existing chiral center(s) on the substituted tropane will create diastereomers (*22*). Indeed, two diastereomers of [^{99m}Tc]TRODAT-1 were obtained in our studies, and the ratio of the diastereomers appears to be constant (*22*). The full characterization of the diastereomers of [^{99m}Tc]TRODAT-1 and the full characterization of the surrogate nonradioactive rhenium complexes have been reported in a separate report (*22*). The isolated

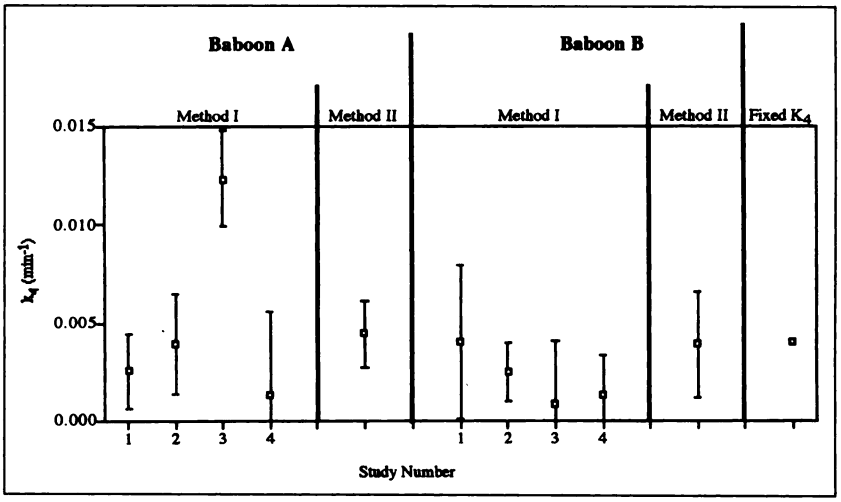

FIGURE 9. Parameter and SEEs for k_4. Fixed value of k_4 = 0.004 min^{-1} was chosen based on results of method II analysis. Both subjects had very similar k_4 values (0.0044 ± 0.0017 and 0.0039 ± 0.0027 for baboons A and B, respectively) using method II.

TABLE 2
Results of Binding Potential Estimates in Both Nonhuman Primate Subjects Using Methods I and II

	Unfixed	Fixed k_4
Baboon A-BP		
Method I-1	189.6	143.5
Method I-2	154.6	153.3
Method I-3	109.0	130.6
Method I-4	578.8	246.1
Average BP (1–3)	151.1	142.5
Method II	133.7	141.4
Baboon B-BP		
Method I-1	124.5	125.6
Method I-2	207.4	152.8
Method I-3	374.0	117.0
Method I-4	202.8	90.0
Average BP (1, 2, 4)	178.2	122.8
Method II	132.5	131.3

Variability of binding potential (BP) estimates was much larger for method I (individualized parameter fitting) than method II (simultaneous fitting). Using fixed $k_4 = 0.004$ min^{-1} yielded more consistent BP estimates than values obtained using no a priori constraints.

Re-diastereomers showed similar binding affinities, with K_i values of 8.4 and 13.8 nmol/L (*22*); however, the corresponding two [^{99m}Tc]TRODAT-1 diastereomers showed different target-to-background ratios and different brain uptakes in rats. These preliminary results indicate that there may exist some in vivo differences in the clearance or metabolism between the two [^{99m}Tc]TRODAT-1 diastereomers.

The [^{99m}Tc]TRODAT-1 used in all of these experiments was a mixture of two diastereomers in a constant ratio. Therefore, the term "apparent" BP is used to represent the data obtained from two diastereomers of [^{99m}Tc]TRODAT-1 in this study. The present studies applied the 3-compartment model based on the assumption of one single species of the tracer used. The excellent convergence of [^{99m}Tc]TRODAT-1 in the estimation of kinetic parameters validated the use of the three-compartment model assuming one ligand. Further experiments will be needed to fully characterize the in vivo kinetics of the individual diastereomers and their contributions to the behavior of the mixture. Because of the nature of the Tc chemistry of a TcO-N_2S_2 center core, it will be a formidable challenge to avoid or eliminate the formation of diastereomers, especially using a kit formulation (i.e., formation of [^{99m}Tc]TRODAT-1 without further purification steps), which is highly desirable for routine clinical application.

The present studies indicate that the apparent BP of [^{99m}Tc]TRODAT-1 can be estimated with dynamic SPECT and arterial blood sampling using analytical solutions to the three-compartment model. Although only two baboons were used in this study, the similarity of the results obtained with the two methods of estimation are very encouraging. The high variability of the BP estimates using method I with no a priori constraints is related to the poor identifiability of model parameters in the individual studies. Poor identifiability of kinetic parameter vectors has been previously described for both PET and SPECT studies using models with no constraints (*30,35–37*). More specifically, the identifiability of k_4 substantially affects the estimation of the BP and kinetic rate constants as shown by decreased variability and SE measurement results on fixing k_4.

In contrast to method I, the BP estimates obtained using method II showed a very minimal change when k_4 was fixed. The identifiability of model parameters using method II was likely improved because only six parameters per subject needed to be estimated given three intrasubject studies. For n intrasubject studies, method I requires the estimation of 4n parameters per study; whereas method II only requires the estimation of n + 3. The ratio of data to model parameters in the limit of increasing n is one model parameter per study using method II versus four model parameters per study using method I.

The use of in vitro values to validate in vivo estimates of similar receptor parameters is complicated by high- and low-affinity binding sites especially observed for DAT protein in vitro, modulation of transporter density during in vitro tissue preparation (*2*), in vivo competition of endogenous dopamine and partial voluming effects from SPECT imaging. However, at present, in vitro data remains the most successful estimate of regional binding potential, receptor density and binding affinity of ligands. Previous studies conducting striatal binding assays in nonhuman primates yielded DAT B_{max} estimates of 459 nmol/L using [^{3}H]CFT (*38*), 478 nmol/L using [^{125}I]β-CIT (*39*) and 760 nmol/L using [^{125}I]IPT (unpublished results). These estimates of the striatal DAT protein density with a 10 nmol/L affinity, estimated from the nonradioactive rhenium complexes of TRODAT-1, yield BP values consistent with the results obtained in this study.

CONCLUSION

The BP and corresponding kinetic rate constants can be reliably estimated in nonhuman primates using [^{99m}Tc] TRODAT-1, a diastereomer mixture, with dynamic SPECT imaging of DATs. The great potential of this novel ^{99m}Tc-based imaging agent to visualize DAT protein in vivo opens new avenues for routine clinical application.

ACKNOWLEDGMENTS

We thank Drs. Lester Rolfe and Vicki Eng, University of Pennsylvania Laboratory Animal Facility, for technical assistance and Ms. Susan West for editorial assistance. This research was supported by grant nos. NS18509 and NS24538 from the National Institutes of Health.

REFERENCES

1. Iversen LL. Role of transmitter uptake mechanisms in synaptic neurotransmission. *Br J Pharmacol.* 1971;41:571–591.
2. Reith MEA, ed. *Neurotransmitter Transporters: Structure, Function, and Regulation.* Totowa, NJ: Humana Press; 1997:405.

3. Giros B, Jaber M, Jones SR, Wightman RM, Caron MG. Hyperlocomotion and indifference to cocaine and amphetamine in mice lacking the dopamine transporter. *Nature.* 1996;379:606–612.
4. Amara SG, Kuhar MJ. Neurotransmitter transporters: recent progress. *Ann Rev Neurosci.* 1993;16:73–93.
5. Fowler JS, Volkow ND, MacGregor RR, et al. Comparative PET studies of the kinetics and distribution of cocaine and cocaethylene in baboon brain. *Synapse.* 1992;12:220–227.
6. Frost JJ, Rosier AJ, Reich SG, et al. Positron emission tomographic imaging of the dopamine transporter with [^{11}C]-WIN35,428 reveals marked declines in mild Parkinson's disease. *Ann Neurol.* 1993;34:423–431.
7. Wong DF, Yung B, Dannals RF, et al. In vivo imaging of baboon and human dopamine transporters by positron emission tomography using [^{11}C]WIN35,428. *Synapse* 1993;15:130–142.
8. Ding Y-S, Fowler JS, Volkow ND, et al. Chiral drugs: comparison of the pharmacokinetics of [^{11}C]d-threo and L-threo-methylphenidate in the human and baboon brain. *Psychopharmacology.* 1997;131:71–78.
9. Innis RB. Single photon emission tomography imaging of dopamine terminal innervation: a potential clinical tool in Parkinson's disease [editorial; review]. *Eur J Nucl Med.* 1994;21:1–5.
10. Seibyl JP, Laruelle MA, Van Dyck CH, et al. Reproducibility of iodine-123-β-CIT SPECT brain measurement of dopamine transporters. *J Nucl Med.* 1996;37:222–228.
11. Mozley PD, Stubbs JB, Kim H-J, et al. Dosimetry of an iodine-123-labeled tropane to image dopamine transporters. *J Nucl Med.* 1996;37:151–159.
12. Tatsch K, Schwarz J, Mozley PD, et al. Relationship between clinical features of Parkinson's disease and presynaptic dopamine transporter binding assessed with [^{123}I]IPT and single-photon emission tomography. *Eur J Nucl Med.* 1997;24:415–421.
13. Abi-Dargham A, Gandelman MS, DeErausquin GA, et al. SPECT imaging of dopamine transporters in human brain with iodine-123-fluoroalkyl analogs of β-CIT. *J Nucl Med.* 1996;37:1129–1133.
14. Neumeyer JL, Tamagnan G, Wang S, et al. N-substituted analogs of 2 beta-carbomethoxy-3 beta-(4'-iodophenyl)tropane (beta-CIT) with selective affinity to dopamine or serotonin transporters in rat forebrain. *J Med Chem.* 1996;39:543–548.
15. Fischman AJ, Babich JW, Elmaleh DR, et al. SPECT imaging of dopamine transporter sites in normal and MPTP-treated rhesus monkeys. *J Nucl Med.* 1997;38:144–150.
16. Innis RB, Seibyl JP, Scanley BE, et al. Single photon emission computed tomographic imaging demonstrates loss of striatal dopamine transporters in Parkinson's disease. *Proc Natl Acad Sci U S A.* 1993;90:11965–11969.
17. Jurisson SS, Berning D, Jia W, Ma D-S. Coordination compounds in nuclear medicine. *Chem Rev.* 1993;93:1137–1156.
18. Hom RK, Katzenellenbogen JA. Technetium-99m-labeled receptor-specific small-molecule radiopharmaceuticals: recent developments and encouraging results. *Nucl Med Biol.* 1997;24:485–498.
19. Tamagnan G, Gao YG, Baldwin RM, Zoghbi SS, Neumeyer JL. Synthesis of beta-CIT-BAT, a potential Tc-99m imaging ligand for dopamine transporter. *Tetrahedron Lett.* 1996;37:4353–4356.
20. Meltzer PC, Blundell P, Jones AG, et al. A technetium-99m SPECT imaging agent which targets the dopamine transporter in primate brain. *J Med Chem.* 1997;40:1835–1844.
21. Meegalla SK, Plössl K, Kung M-P, et al. Synthesis and characterization of Tc-99m labeled tropanes as dopamine transporter imaging agents. *J Med Chem.* 1997;40:9–17.
22. Meegalla SK, Plössl K, Kung M-P, et al. Specificity of diastereomers of [^{99m}Tc]TRODAT-1 as dopamine transporter imaging agents. *J Med Chem.* 1998;41:428–436.
23. Kung HF, Kim H-J, Kung M-P, Meegalla SK, Plössl K, Lee H-K. Imaging of dopamine transporters in humans with technetium-99m TRODAT-1. *Eur J Nucl Med.* 1996;23:1527–1530.
24. Kung M-P, Stevenson DA, Plössl K, et al. [^{99m}Tc]TRODAT-1: a novel technetium-99m complex as a dopamine transporter imaging agent. *Eur J Nucl Med.* 1997;24:372–380.
25. Laruelle M, Wallace E, Seibyl JP, et al. Graphical, kinetic, and equilibrium analyses of in vivo [^{123}I]beta-CIT binding to dopamine transporters in healthy human subjects. *J Cereb Blood Flow Metab.* 1994;14:982–994.
26. Wong DF, Gjedde A. Compartments and reaction volumes of brain fluid spaces: shaken, not stirred. *J Nucl Med.* 1996;37:126–127.
27. Delforge J, Syrota A, Bendriem B. Concept of reaction volume in the in vivo ligand-receptor model. *J Nucl Med.* 1996;37:118–125.
28. Kushner SA, McElgin WT, Mozley PD, Kung HF. A fully-automated method of multi-modal coregistration using external fiducial markers [Abstract]. *J Nucl Med.* 1996;37:990P.
29. Mintun MA, Raichle ME, Kilbourn MR, Wooten GF, Welch MJ. A quantitative model for the in vivo assessment of drug binding sites with positron emission tomography. *Ann Neurol.* 1984;15:217–227.
30. Abi-Dargham A, Laruelle M, Seibyl J, et al. SPECT measurement of benzodiazepine receptors in human brain with iodine-123-iomazenil: kinetic and equilibrium paradigms. *J Nucl Med.* 1994;35:228–238.
31. Larvelle M, Abi-Dargham A, Al-Tikriti MS, et al. SPECT quantification of [I-123]iomazenil binding to benzodiazepine receptors in nonhuman primates. 2. Equilibrium analysis of constant infusion experiments and correlation with in vitro parameters. *J Cereb Blood Flow Metab.* 1994;14:453–465.
32. Phelps ME, Huang SC, Hoffman EJ, Selin C, Solokoff L, Kuhl DE. Tomographic measurement of local cerebral glucose metabolic rate in humans with (F-18)2-fluoro-2-deoxy-D-glucose: validation of method. *Ann Neurol.* 1979;6:371–382.
33. Levenberg K. A method for the solution of certain problems in least squares. *Quant Appl Math.* 1944;2:164–168.
34. Kung M-P, Plössl K, Meegalla SK, Kung HF. A kit formulation for the preparation of [^{99m}Tc]TRODAT-1: a new dopamine transporter imaging agent [Abstract IV-23]. *Proc XIIth Int Symp Radiopharm Chem,* Uppsala, Sweden. 1997;40:263–265.
35. Carson RE. The development and application of mathematical models in nuclear medicine. *J Nucl Med.* 1991;32:2206–2208.
36. Frost JJ, Douglass KH, Mayberg HS, et al. Multicompartmental analysis of [^{11}C]carfentanil binding to opiate receptors in humans measured by positron emission tomography. *J Cereb Blood Flow Metab.* 1989;9:398–409.
37. Abi-Dargham A, Gandelman M, Zoghbi SS, et al. Reproducibility of SPECT measurement of benzodiazepine receptors in human brain with iodine-123-iomazenil. *J Nucl Med.* 1995;36:167–175.
38. Madras BK, Spealman RD, Fahey MA, Neumeyer JL, Saha JK, Milius RA. Cocaine receptors labeled by [^{3}H]2β-carbomethoxy-3β-(4-fluorophenyl)tropane. *Mol Pharmacol.* 1989;36:518–524.
39. Laruelle MA, Giddings SS, Zea-Ponce Y, et al. Methyl 3beta-(4-[^{125}I]iodophenyl) tropane-2beta-carboxylate in vitro binding to dopamine and serotonin transporters under "physiological" conditions. *J Neurochem.* 1994;62:978–986.